UC Berkeley
UC Berkeley Previously Published Works

Title
Upward flame spread over corrugated cardboard

Permalink
https://escholarship.org/uc/item/4mj6s3nn

Journal
Combustion and Flame, 158(7)

ISSN
0010-2180

Authors
Gollner, MJ
Williams, FA
Rangwala, AS

Publication Date
2011-07-01

DOI
10.1016/j.combustflame.2010.12.005

Peer reviewed

Upward Flame Spread Over Corrugated Cardboard

M.J. Gollner[a,*], F.A. Williams[a], A.S. Rangwala[b]

[a]*University of California, San Diego, Department of Mechanical and Aerospace Engineering.*
9500 Gilman Drive, La Jolla, CA 92093-0411.
[b]*Worcester Polytechnic Institute, Department of Fire Protection Engineering.*
100 Institute Road, Worcester, MA 01609-2280

Abstract

As part of a study of the combustion of boxes of commodities, rates of upward flame spread during early-stage burning were observed during experiments on wide samples of corrugated cardboard. The rate of spread of the flame front, defined by the burning pyrolysis region, was determined by visually averaging the pyrolysis front position across the fuel surface. The resulting best fit produced a power-law progression of the pyrolysis front, $x_p = At^n$, where x_p is the average height of the pyrolysis front at time t, $n = 3/2$, and A is a constant. This result corresponds to a slower acceleration than was obtained in previous measurements and theories (e.g. $n = 2$), an observation which suggests that development of an alternative description of the upward flame spread rate over wide, inhomogeneous materials may be worth studying for applications such as warehouse fires. Based upon the experimental results and overall conservation principles it is hypothesized that the non-homogeneity of the cardboard helped to reduce the acceleration of the upward spread rates by physically disrupting flow in the boundary layer close to the vertical surface and thereby modifying heating rates of the solid fuel above the pyrolysis region. As a result of this phenomena, a distinct difference was observed between scalings of peak flame heights, or maximum "flame tip" measurements and the average location of the flame. The results yield alternative scalings that may be better applicable to some situations encountered in practice in warehouse fires.

Keywords: Upward Flame Spread, Warehouse Fires, Corrugated Cardboard

Nomenclature

α Entrainment coefficient

ΔH_c Heat of combustion per unit mass of fuel consumed

$\dot{m}'$ Mass-loss rate per unit width

$\dot{q}''$ Time-dependent heat flux per unit area

$\dot{Q}'$ Heat-release rate per unit width

*Corresponding author
Email address:* `mgollner@ucsd.edu` (M.J. Gollner)

ρ	Density of solid fuel
ρ_f	Average gas density in the flame
ρ_a	Density of ambient air
τ	t'/t
A	Constant in x_p correlation
a	Average horizontal distance over which oxygen diffuses
B	Constant in x_f correlation
C	Constant in $\dot{q}''$ correlation
c	Heat capacity per unit mass
D	Molecular diffusion coefficient
f	Stoichiometric fuel-to-air mass ratio
g	Acceleration of gravity
k	Thermal conductivity
n	Power-law correlation exponent
T	Surface temperature
t	Time
T_0	Initial temperature
T_p	Pyrolysis temperature
u_z	Average vertical velocity
x_f	Flame height
x_p	Pyrolysis height
y_f	Flame standoff distance

1. Introduction

The work reported here was motivated by a study of the flammability properties of stored warehouse containers, as part of an effort to develop a rational basis for assessing the flammability or relative fire hazards of these containers. In a warehouse setting, these containers or "commodities" are stacked to heights sometimes exceeding 15 meters, in facilities with enormous floor area, creating a dangerous environment with large sources of fuel that are difficult for emergency personnel to reach. Detrimental effects of recent warehouse fires have included deaths of firefighters, damage to local environments, and harsh economic penalties for building owners and insurance interests, even in facilities fully protected to modern codes and standards

[1–3]. Compounding this risk potential in these occupancies is the flat, upright configuration of stored goods and their arrangement which creates exceptionally long vertical flue spaces. This configuration exhibits high rates of fire spread, especially enhanced within flue spaces where the flow is channeled and radiates, producing longer flames.

A key aspect of characterizing the flammability of a group of vertically stored materials is to predict the relative rates of upward spread. We have performed experiments involving a corrugated cardboard carton containing crystalline polystyrene cups. This constitutes a standard item used for sprinkler testing in the fire-protection industry [3]. Distinct stages of burning were identified, first involving the outer corrugated cardboard alone, then inner packaging material, and last the stored polystyrene as well [4]. It is during the first stage of this burning, involving upward spread over a vertical surface of corrugated cardboard, that the greatest potential for extinguishing a warehouse fire initatied by this type of combustion presents itself. Predicting the time necessary for flames to spread upwards, and thus the duration of this critical initial period of fire growth (often lasting only 1–2 minutes) is therefore an important component of classifying the hazards of commodities and developing a general model of fire growth in warehouse configurations. Spread behavior during this initial period of fire growth is the topic of the investigation reported here.

2. Steady Wall Flames

Upward flame spread along vertical solid combustible surfaces occurs as a consequence of heat transfer from the flames to the unignited fuel. Heights of flames adjacent to burning fuel surfaces therefore are important in upward spread. Kosdon et al. [5] and later Kim et al. [6] developed similarity theories to describe laminar boundary-layer combustion adjacent to a vertical flat plate, employing experimental data on vertical cylinders to support the similarity hypothesis. More recent theoretical work has addressed additional phenomena, such as oxygen leakage leading to flame extinction [7]. Flame heights from such steady-burning theories can be deduced by evaluation of the maximum height of the stoichiometric surface, and a method for estimating transfer numbers experimentally for spreading flames by using the similarity solutions has been reported [8]. Buoyancy causes this height to extend above the maximum height of the pyrolyzing fuel. Pagni and Shih [9] refined the description of the combusting plume and termed *excess pyrolyzate* the gaseous fuel present above the height of the pyrolyzing surface. An increase in the mass of the excess pyrolyzate increases the flame height, thereby increasing rates of upward flame spread in wall fires. These authors formulated and solved conservation equations in the region numerically. Later, Annamalai and Sibulkin [10] obtained approximate analytical solutions to the laminar boundary-layer equations from Pagni and Shih's formulation for the flame height and flame spread rates by assuming polynomial profiles.

Most of these papers also report experimental results. Numerous experiments [11–20] have been performed subsequently on steady-burning wall flames using both solid fuel surfaces and gaseous line and wall-fire burners to investigate relationships among flame heights, burning rates, and incident heat fluxes. Among the most thorough work, Ahmad and Faeth [11] performed such experiments in the turbulent regime on steadily burning, vertical fuel-soaked wicks and compared their results to numerical solutions of boundary-layer equations. Their work established a unified correlation of laminar and turbulent burning-rate measurements for steady wall fires on the basis of a modified Froude Number.

Delichatsios hypothesized a simplified flame-height correlation on the basis of dimensional analysis, suggesting that the flame height depends only on the total heat-release rate per unit

3

width of a wall fire [12, 21]. This relationship,

$$x_f \sim (\dot{Q}')^{2/3}, \tag{1}$$

has been observed (with $\dot{Q}'$ in the range of 20–100 kW/m^2) during experiments on gaseous line burners [13–15], gaseous wall-fire burners [11, 12, 17–20] and vertical samples of solid polymethyl methacrylate (PMMA) and wood at varying levels of external heat flux [13, 15, 16, 18], although earlier results of Markstein and de Ris [22] suggested a power of 1/2 instead, so some differences in exponents may be encountered.

To understand the basis of equation 1, consider a turbulent wall plume with an entrainment coefficient α, the local ratio of the tangential velocity of incoming air to the average upward velocity in the plume. If f denotes the mass of fuel required to react with a unit mass of air, that is, the stoichiometric fuel-to-air mass ratio, then a mass balance indicates that the burning rate per unit width can be represented as

$$\dot{m}' = f x_f \alpha \rho_a u_z, \tag{2}$$

where x_f is the flame height, ρ_a the density of ambient air, and u_z the average vertical velocity, which can be estimated as $u_z = \sqrt{x_f g}$ for a buoyant plume, where g is the acceleration of gravity [1]. The basis of the simple estimate in equation 2 should be self-evident since the factor multiplying f on the right-hand side is just the product of the average horizontal mass inflow rate per unit area with the height of that area. Similar reasoning could be applied to a vertical axisymmetric jet for which the total mass flow rate would be given by including as as an additional geometrical factor on the right-hand side, the jet circumference. Solving for the flame height reveals the scaling

$$x_f = [\dot{m}'/(\rho_a \alpha f \sqrt{g})]^{2/3}, \tag{3}$$

which leads to equation 1 because the heat-release rate per unit width for steady burning, $\dot{Q}'$ is the product of the fuel mass-loss rate per unit width, $\dot{m}'$ and the heat of combustion per unit mass of fuel consumed, ΔH_c.

While equation 1 has strong experimental support for large turbulent wall flames, having $\dot{Q}' > 30$ kW/m^2, recent experimental results in a range of lower heat fluxes have suggested a change in the steady relationship between heat-release rates and flame heights for tests below approximately 20 kW/m^2. Tsai and Drysdale [20] performed experiments on vertical PMMA samples and a gas-fired burner with several mounting configurations and for all samples found a distinctly linear relationship between total heat-release rates and flame heights when $\dot{Q}'$ was less than 20 kW/m^2. It is reasonable that the dependency of x_f on $\dot{Q}'$ should be stronger at these smaller scales. If the flow is laminar, then the oxygen reaches the reaction zone by molecular diffusion, and in equation 2, the inflow velocity αu_z should then be replaced by a diffusion velocity, D/a, where D is a molecular diffusion coefficient, and a is an average horizontal distance over which oxygen diffuses. As was pointed out by Roper [24], this horizontal distance can be estimated as an average volume flow rate per unit width, $\dot{m}_f/(f\rho_f)$ (where ρ_f is an average gas density in the flame), divided by an average buoyant velocity, $\sqrt{x_f g}$. Substitution of these estimates into equation 2 yields

---

[1] A factor neglected here is the difference between the plume and ambient densities, divided by the ambient density, because this ratio is close enough to unity [23].
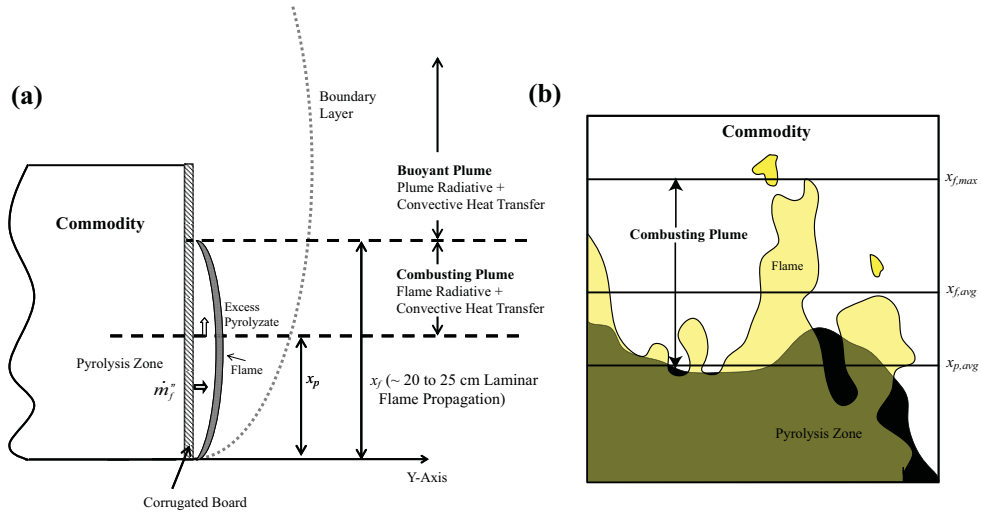
Figure 1: (a) Theoretical description of 2-D upward flame spread [4]. (b) Description of measured flame and pyrolysis heights observed from a representative front video frame. As shown in the figure, $x_{f,max}$ is defined as the top of an attached yellow flame, $x_{f,avg}$ the mean height of the flame across the sample width, and $x_{p,avg}$ the mean height of the pyrolysis front across sample width.

$$x_f = (\dot{m}'_f)^{4/3}/(\rho_f \rho_a f^2 D \sqrt{g})^{2/3} \qquad (4)$$

in place of equation 3, which would yield

$$x_f \sim (\dot{Q}')^{4/3} \qquad (5)$$

in place of equation 1. Since the flow, however, is unlikely to be perfectly laminar, a result intermediate between equations 1 and 5 may be expected. In fact, Tsai and Drysdale [20] reported exponents of 0.98 to 1.25, depending on sample mounting, in their relationship between heat-release rates and flame heights.

3. Upward Flame Spread

The general model for upward flame spread, represented graphically in figure 1a, consists of three primary regions, the pyrolysis zone, extending to height x_p, where ignited material burns and contributes fuel to rising flames, the combusting plume, the region $x_f - x_p$, where unburnt fuel (excess pyrolyzate) from the pyrolyzing zone continues to burn and heat unignited solid fuel, and a buoyant plume above x_f carrying combustion products and entrained air above the combustion region. The spread process is driven by the heat flux from the flame to unignited material above the pyrolysis front [25]. Because the rate of upward flame spread is nearly always orders of magnitude larger than that of downward or lateral flame spread, these processes can often be neglected in the analysis of upward flame-spread scenarios.

Even when edge effects are irrelevant, so that the vertical combustible sample effectively is of infinite width (as in the present study), a wide variety of upward spread behavior can occur, depending upon the nature of the combustible material [26] and the vertical dimension of the

5

surface. Much attention has been devoted to thermoplastics, PMMA being the material investigated most widely. For such materials, when the flames are small and laminar, the spread rate from both theory and experiment for thermally thick materials obeys $x_p \sim t^2$ [27–29] (although one set of experimental results [28] correlates better with $x_p \sim t^{1.7}$), but when the flames are large and turbulent, x_p increases exponentially with time [27, 30, 31]. Cellulosic materials generally behave quite differently. At small scales, for thermally thick materials, it has proven to be difficult to achieve reasonable accuracy in determining the functional dependence of x_p on t, the results being sensitive to the manner of initiations and the type of cellulosic. A simple linear dependence, $x_p \sim t$, appears to apply for wood, within the accuracy of the data [30, 32, 33]. At later times, unless the material is sufficiently thin that burnout at the bottom become important [33] (leading finally to a constant upward spread rate), char eventually builds up to such an extent that upward spread stops, and self-extinguishment occurs [30, 33]. Sufficiently intense external radiation can, however, lead to continued spread [33, 34]. For corrugated cardboard with a minimal ignition stimulus under a typical kind of warehouse-fire condition, the present work will yield improved accuracy for the exponent n in a relation $x_p \sim t^n$.

Upward flame spread is quite complex. Models must address the burning rate of the fuel below x_p, the time-dependent temperature field in the condensed phase above x_p, and the heat flux from the gas to the solid above x_p. Even the simplest solid materials that experience only time-dependent heat conduction up to a fixed surface temperature required for ignition, thereby being readily amenable to an approximation of a constant heating time for ignition during upward spread, in general must be described by difference-differential equations [22], which predict a stepwise, "leapfrogging" spread [27] that can approach continuous spread behavior, describable by ordinary differential equations [30] only at long times [22, 30]. When charring is important, more complicated descriptions of the behavior of the fuel in response to the heating above x_p are needed [30]. Under the conditions of the experiments investigated here, charring of the cellulosic corrugated cardboard is mild, providing a good indication of the arrival of the pyrolysis front (by observing blackening of the face), but not extending significantly above the pyrolysis front to impede spread. In addition, while burnout at the bottom of the cardboard begins towards the end of the upward-spread tests, it is not extensive enough to necessitate its inclusion in the description of the spread, and, moreover, the soon-to-follow involvement of combustion of the commodity [4] overpowers the effects of burnout in the fire history.

Because of the overall complexity of the upward spread process, simplifications of the description of the spatial dependence of the heat flux from the gas to the solid above x_p are prevalent in the literature. The gas flow in that region, involving combustion of the excess pyrolyzate, is complicated and not amenable to similarity approximations with a high degree of accuracy, even for laminar flow. In early work, Sibulkin and Kim [35] assumed a constant heat flux to the wall between x_p and x_f and a flux decaying exponentially with height in the nonreacting plume above x_f, but in later work, Annamalai and Sibulkin [10] ignored this exponential tail, employing only a constant heat flux over the distance $x_f - x_p$, an approximation that is very common elsewhere in the literature [22, 30, 33]. A considerable amount of information actually is available on heat fluxes to walls as functions of height above the burning area in wall fires, and such detailed information has been employed in numerical algorithms calculating upward flame spread [31]. Full numerical simulations are beginning to appear more frequently now [36, 37]. Simplified models of the spread process that make rough approximation ignoring these details generally invoke a constant heat flux between x_p and x_f and zero heat flux above x_f, assuming that the shape of the heat-flux distribution will not affect the predictions significantly. We have found, however, that we cannot correlate our experimental results on the basis of such an assumption. Instead, a

6

power-law variation of the heat flux with height is needed.

From the one-dimensional time-dependent heat-conduction equation for a semi-infinite solid of density ρ, heat capacity per unit mass c and thermal conductivity k, it can be shown that with heating at the surface by a time-dependent heat flux per unit area $\dot{q}''$, beginning with a uniform temperature T_0 at time zero, the surface temperature T at time t is given by [31]

$$T = T_0 + \frac{1}{\sqrt{\pi k \rho c}} \int_0^t \frac{\dot{q}''}{\sqrt{t - t'}} dt'. \tag{6}$$

If the material begins to pyrolyze at a fixed pyrolysis temperature T_p, then by introducing the nondimensional variable $\tau = t'/t$, it becomes clear that the integral

$$I = \int_0^1 \frac{\dot{q}'' \sqrt{t}}{\sqrt{1 - \tau}} d\tau \tag{7}$$

must be a constant, determined by the material properties. Under the assumption that the heat-flux distribution above the pyrolysis zone has the power-law variation

$$\dot{q}'' = C/x^{1/3}, \tag{8}$$

equation 7 implies that the time t of arrival of the pyrolysis front will obey

$$x_p = At^{3/2}, \tag{9}$$

where A is a constant. Under the approximation that the flame height x_f is proportional to the burning rate per unit width $\dot{m}'$ and that $\dot{m}'$ is proportional to x_p, this result also yields

$$x_f = Bt^{3/2}, \tag{10}$$

where B is a constant. These variations will be seen to fit the present data best. It may be noted that, with heat transfer controlled by convection, equation 8 implies a boundary-layer thickness that increase with height in proportion to $x^{1/3}$, which is in contrast with the classical similarity solution for natural convection, giving an $x^{1/4}$ dependence and $x_p \sim t^2$. The reasons for this difference will be discussed after the experimental results are presented.

4. The Experiments

The surface tested was the front face of a package of single-walled corrugated cardboard of dimensions $530 \times 530 \times 510$ mm. The inside of the carton was compartmentalized by corrugated cardboard dividers to create cells containing polystyrene cups. Other details of the overall experiment are available elsewhere [4] but are not relevant to the present study. Measurements addressed in this study were restricted to flame spread over the first 30 cm of the front surface, so that exposure of the interior of the commodity, burnout, and spread over the rear surface of the cardboard have not yet begun. Moreover, since the sample width exceeded 500 mm, effects of the width on flame heights and on upward spread, which have been addressed in the literature (much of it recent) [17, 19, 20, 38–41] need not be considered here; the width no longer plays a role when it is greater than about 300 mm [38, 41] so that, during the portion of the overall experiment considered here, the cardboard face is effectively of infinite width. The front face was made of approximately 3 mm thick single-ply corrugated cardboard (a schematic diagram of
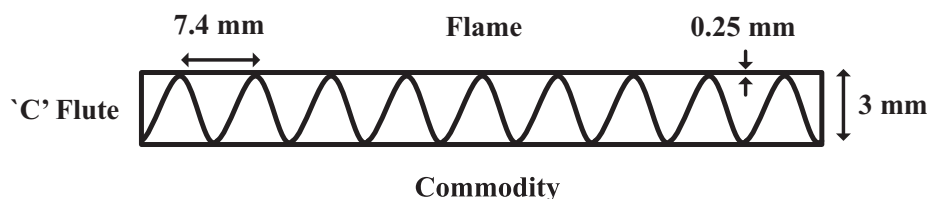
7

Figure 2: Cross-section of 'C' Flute corrugated cardboard [33, 42] used in the experiments.

which is shown in figure 2) with its flues oriented vertically. The gross density of the corrugated board has been reported as 0.12 g/cm^3, and the top layer paper density 0.48 g/cm^3 [42].

The package was placed on top of a load cell that measured mass with an accuracy of ±0.5 g. A Sony HD digital camcorder recording at 29.97 fps was positioned in front of the test apparatus to record flame heights and to visually observe the progression of the pyrolysis front. A digital SLR camera was also positioned on the side of the apparatus to record the flame shape close to the fuel surface. The setup was placed under a 1 MW hood to capture burning fumes and embers. Ignition was achieved by adding 4 mL of n-heptane to a strip of glass fiber board approximately 1 cm tall, 0.35 m wide by 3 mm in depth. The wetted wick igniter was held by an aluminum u-channel that was positioned adjacent to and below the lower front edge of the commodity. The video cameras and a data acquisition system used to record load cell readings were started before ignition of the commodity. The data acquisition system and camcorders were synchronized with a stopwatch used to determine the offset between instrument start time and ignition start time. Experimental time begins when the strip is piloted at the centerline of the commodity's front face.

5. Experimental Results

5.1. Flame Heights

Experimentally, the simplest method of determining flame heights has been by marking a ruler on the side of a combustible sample, and observing the arrival of the flame at set markers to determine the flame height, as was done in the work of Tewarson and Ogden [16]. Similar methods have been used by Orloff et al. [27] and by Tsai [40]. Saito et al. determined flame heights by inspecting regularly time-spaced frames from front video footage and reasoned that this method is analogous to performing measurements at every frame obtained [30]. Fernandez-Pello [28] used shutter settings with still photography to resolve flame heights, a somewhat manual method to average over the effects of flame intermittency. To increase precision, Audouin et al. [43], Rangwala et al. [38] and Consalvi et al. [44] all applied thresholds of video images to determine the extent of the flame. Consalvi et al. also related the flame height to the heat flux imparted to a solid by comparison with a numerical model of the process.

Visual assessments of flame locations were performed in the present work as the flame spread up the front face of corrugated cardboard to approximately 30 cm in height. Frames from front video during upward flame spread were imported into Matlab, and then the location of the flame was visually selected utilizing zoomed video frames at 15 points across the width of the front face and recorded by computer software. The height of the flame front at each position was defined as the peak of the visible yellow flame at that location. Although a threshold could be implemented for flame heights, it was found to make little difference in the results.
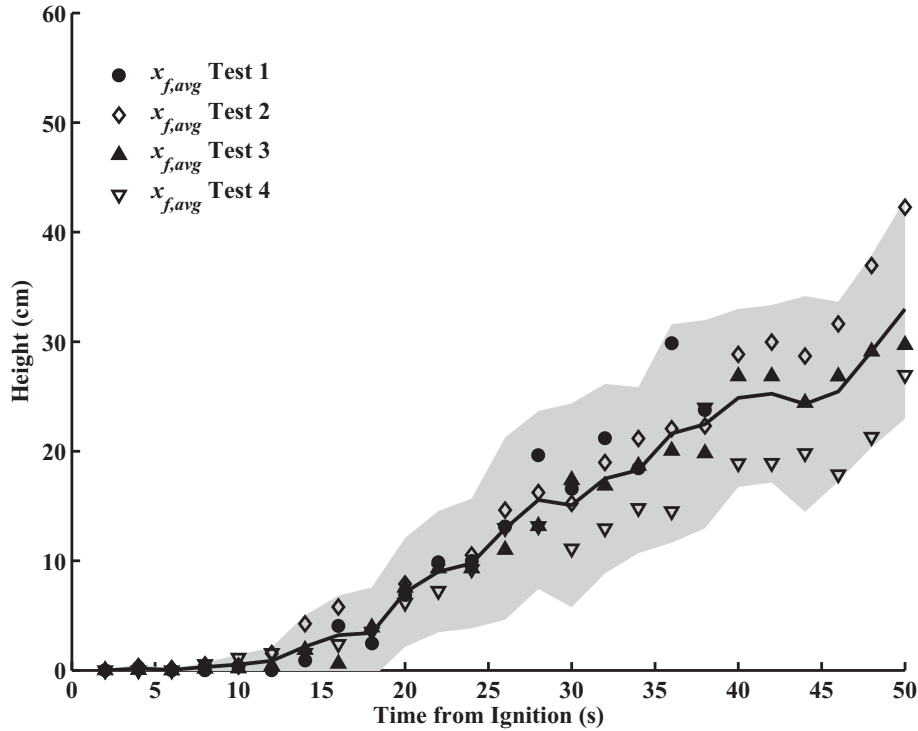
8

Figure 3: Flame heights for four tests assessed visually across the width of the front face of corrugated cardboard. Points represent averages over the horizontal distance for each test, the line is the average of all the tests, and the shaded region defines boundaries of the standard deviation.

Averaged flame heights from four tests are shown in figure 3. Deviations in the flame height across the width of the sample are indicated by a shaded gray region above and below these points. The turbulent fluctuating nature of flames causes significant scatter, indicated by an increasing region of deviation over time. Although fluctuations could be decreased by using more uniform materials, such as PMMA, or by introducing sidewalls to limit entrainment effects that disturb the flow, that would exclude the real-world effects of interest here. The growth of the deviations throughout time is important, and observation of these deviations aids in the understanding of early-stage upward fire propagation over practical cellulosic materials. Time-averaging of video frames, as is often performed in steady pool-fire experiments, cannot be applied usefully to these quickly spreading flame fronts.

Despite the significant scatter of flame heights, averaged values of flame heights were similar for all four tests. This suggests that the small-scale behavior of the flame is repeatable when averaged. This average flame height is representative of the average vertical extent of the combusting plume, which is the region that imparts the main heat flux to the virgin solid fuel ahead of the flame. The flame tip, or maximum flame height seen anywhere across the width of the face, is less representative of the average heat-flux region, but it is shown in figure 4 since it has often been referred to as the "flame height" in previous studies and therefore is useful for comparisons [44]; it is noticeably (perhaps 50 %) higher than the average shown in figure 3, but the differences
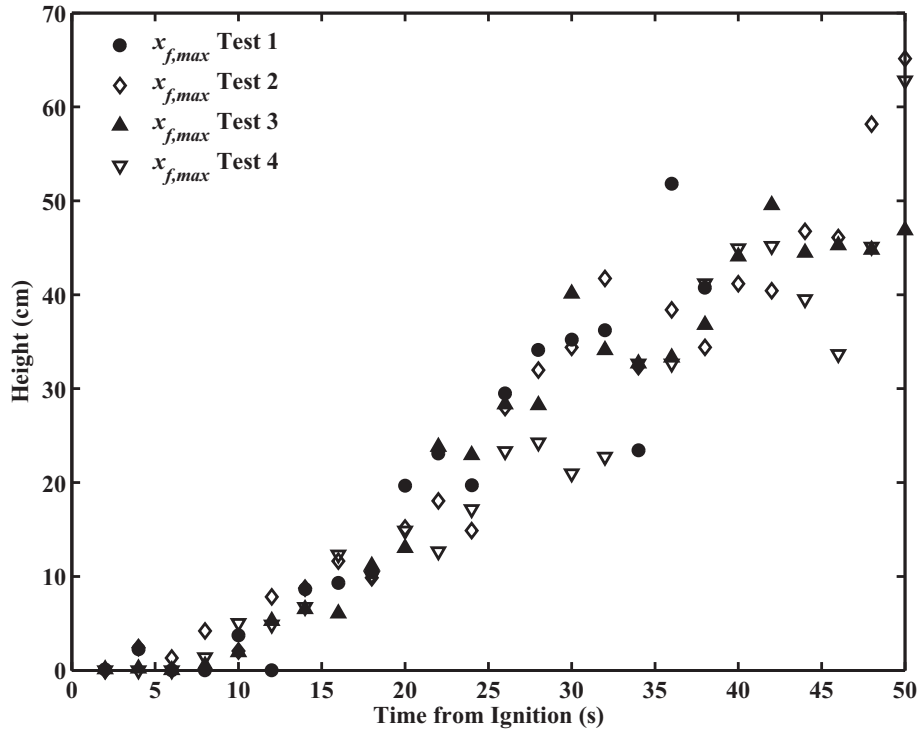
Figure 4: Maximum or flame-tip heights, measured as the peak of attached yellow flames at each time step for four tests. Errors are not shown in the figure because single values were selected for each test, but estimated magnitudes of errors in the selection technique are 3–4 cm.

would be much less in more uniform, idealized experiments.

Average and maximum flame heights for all four tests were averaged, shown together in figure 5. Deviations between averaged values from the tests are now indicated by a shaded gray region above and below sampled points. Both flame heights follow a similar trend. To aid in assessment of analytical models and to generate empirical results, various fits to the experimental data are investigated. From figure 5 it can be seen that a power-law fit, $x_f = Bt^n$, with $n = 3/2$, agrees best with the data, a conclusion further supported by the log-log plot and more detailed information in the appendix.

5.2. Burning-Rate Relationships

Scaling analyses presented in section 2 relate flame heights to fuel mass-loss rates for steadily burning wall fires. Characteristic gas-phase flow times are short enough compared with spread rates that quasi-steady approximations should be reasonable. Fuel mass-loss rates, $\dot{m}$, were determined by differentiating polynomial fits to mass-loss data collected by a load cell at the base of the experimental apparatus. Additional details of the methods used for the mass-loss data, including the original data, can be found elsewhere [4, 45]. Fuel mass-loss rates were then converted into heat-release rates per unit width, $\dot{Q}' = \dot{m}\Delta H_c/w$, where w denotes the width of the sample, and the heat of combustion ΔH_c was assigned the constant value 13.2 kJ/g, associated
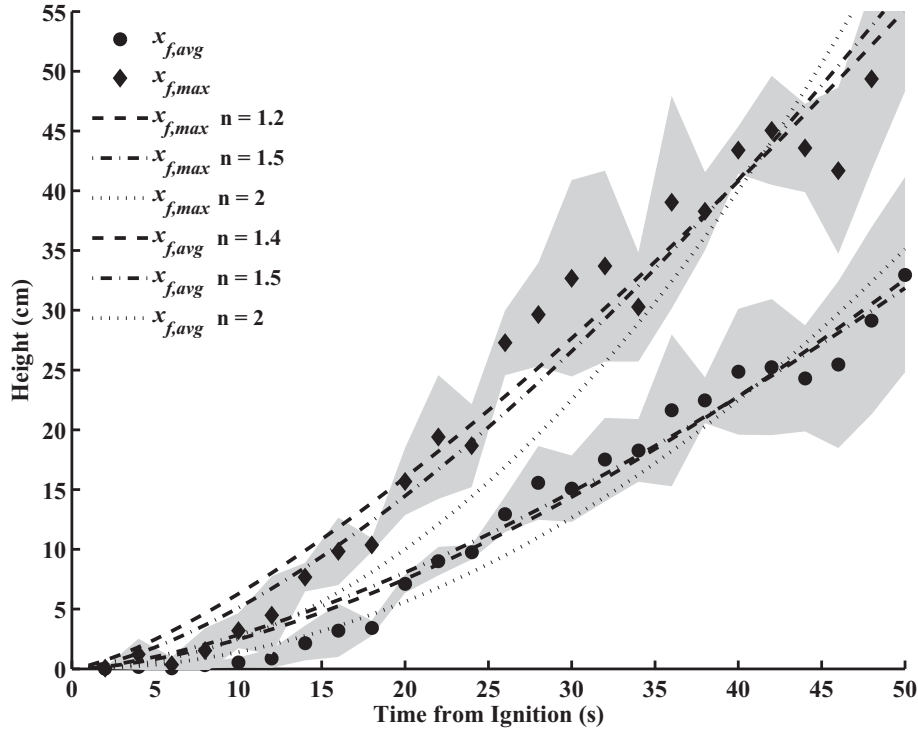
10

Figure 5: Averaged flame heights and maximum flame heights combined for all four tests. Deviations between the maximum or average value for each test are denoted by a shaded gray region above and below test points. Unlike the shaded region in figure 3, the shading here refers only to the standard deviation between the averaged values of the four runs. Power-law fits to experimental data are also shown as dashed lines.

with corrugated cardboard [46]. Figure 6 displays the resulting relationship between the heat-release rates and both average and maximum flame heights.

In figure 6, vertical and horizontal error bars around each experimental point indicate the range of values of the flame height and the heat-release rate, respectively between the four experimental tests. The data points shown represent the average between these tests, and least-squares fitting was applied to these average values to derive correlations in terms of power-law functions. The best-fit power-law function for the average flame height was found to have an exponent of 1.1, with an R^2 value of 0.99, and the maximum flame-height data were found to have an exponent of 0.9, with an R^2 value of 0.98. Within a 95% confidence interval, the exponent of the average flame height data could lie between 1.0 and 1.3, and the exponent of the maximum flame height data could lie between 0.8 and 1.0. Fits to the averaged experimental data, therefore, suggest an exponent of unity, within the accuracy of the measurements.

Some of the flame-tip results from the literature also are shown in figure 6. The power law [12] most strongly supported in the literature for $\dot{Q}' > 20$ kW/m^2 is seen to lie well within the results of the presented data in that range but to predict heights above our error limit at lower values. The linear correlation of steady-burning measurements [20] for $\dot{Q}' < 20$ kW/m^2 is
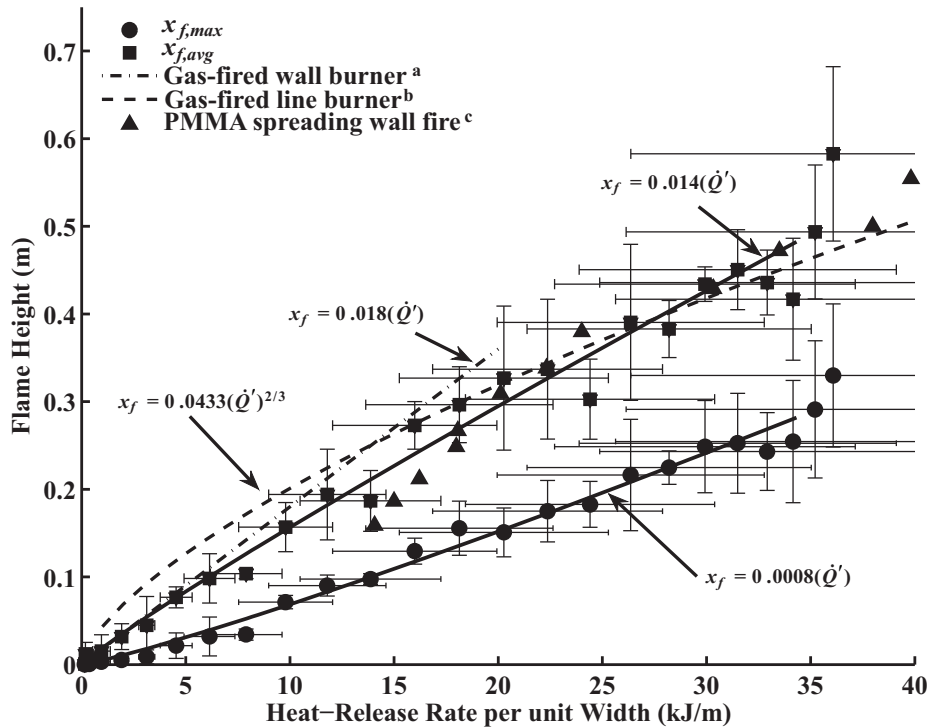
Figure 6: Maximum flame heights (flame tips) and flame heights averaged across the width of the front face as functions of the heat-release rate. Errors (increasing over time) for flame heights and heat-release rates are shown as vertical and horizontal error bars, respectively. Solid lines are linear least-squares fits, and flame-tip results from the literature are shown for [a]Gas-fired wall burner [20] (dot-dash curve), [b]Gas-fired line burner [12] (dashed line), [c]PMMA spreading wall fire [20] (triangles).

consistent with our data there but would begin to fall above our error limit at the highest heat-release rates. The somewhat lower slope of our best-fit linear correlation for $\dot{Q}' < 40$ kW/m^2 is seen in figure 6 to encompass, within error estimates, data [20] on upward spreading wall fires. In the size ranges of our experiments, there thus may be a small tendency for flame-tip heights to fall below the best steady-burning correlations. It becomes clear from the results in figure 6 that, in addressing the average flame heights most relevant to average spread rates, a linear correlation with a slope significantly less than that of the best available correlation in the literature for idealized experiments is needed. This smaller slope seen in figure 6 is employed in the following considerations.

5.3. Pyrolysis Heights

Because corrugated cardboard distinctly changes in color from light brown to black once charring occurs, the pyrolysis front location is easy to distinguish visually at each time step. Frames from front video during upward flame spread were imported into Matlab, and then the location of the pyrolysis front was visually selected along 15 points across the width of the front face and recorded by computer software. In some cases, one or two points on the edge of the
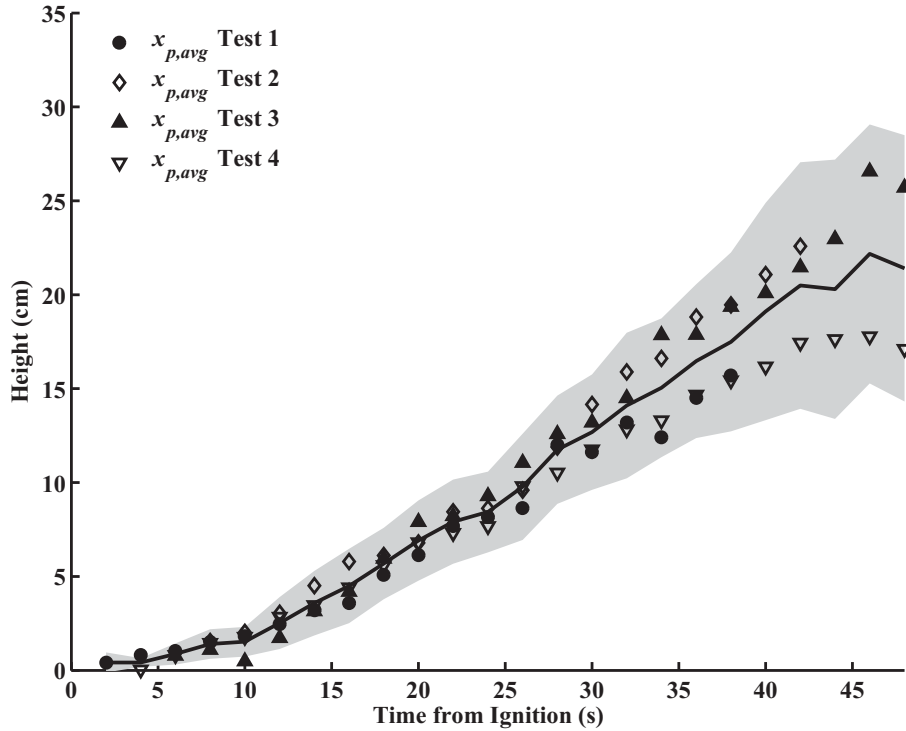
Figure 7: Pyrolysis heights for four tests assessed visually across the width of the front face of corrugated cardboard and averaged. Deviations between measurements across the face are indicated by a shaded gray region above and below experimental measurements.

sample did not ignite and thus were not pyrolyzing; these points were therefore neglected for the entire test. A section of at least the middle 35–40 cm remained uniformly spreading and therefore was analyzed for the duration of all four tests.

Spatially averaging the measured locations of the pyrolysis front across the width of the front face results in a mean pyrolysis height, shown in figure 7. Despite the uniform ignition at the base of the front face, natural deviations in the makeup of the cardboard, the onset of turbulence, entrainment, and other real-world effects on this wide surface result in advancement of the front that is not entirely uniform. The deviations between the averaged heights measured across the width of the sample for each time step are indicated by a shaded gray region above and below the averaged values. These deviations grow over time, as the onset of turbulence occurs and smaller deviations from earlier in the tests grow in magnitude,and they cannot be avoided without artificially modifying the test apparatus. The average values shown are of interest for testing spread-rate models.

Analyzing captured video footage through computer software, such as by distinguishing thresholds between unburned and burnt material in theory could be an improved method of analysis, although it proved to be unnecessarily complicated. Flames fluctuated, partially obscuring views of the pyrolysis front, and smoke and charred pieces caused an initial test of using a threshold to determine pyrolysis heights to be exceedingly inaccurate. Therefore, the simpler,

13

though more labor-intensive process of manually selecting the pyrolysis location was implemented. Other methods, such as using a 10.6 micrometer bandpass filter on an infrared imaging camera, as Arakawa et al. [47] did, could be ideal and facilitate threshold analysis of data by removing influences of the flame and detecting temperature change along the solid fuel surface. In view of the limited resolution and large expense of such equipment, however, visual imaging was deemed sufficient for these small-scale measurements.

The average or mean pyrolysis front location for all four tests was determined by averaging the locations from each test and is shown in figure 8. Deviations across the front face in each of four tests were combined with deviations between tests and are presented as a shaded gray region in figure 8. Just as in data for each individual test, errors grow slightly as time progresses and deviations both across the face and between tests occur. A maximum height of the pyrolysis front, indicating the highest point advancement across the front, averaged across four tests is also shown as a line above the average pyrolysis heights. It is seen from figure 8 that this maximum value almost precisely follows the peak of the standard deviation bars above the average pyrolysis heights. This indicates that the range in which pyrolysis heights exist at each time step is fairly small, within the vertical error bars, and analysis of the peak pyrolysis height does no more than represent the maximum deviations present. It thus is not analyzed further in this study. A similar exercise could be conducted (with similar results) for the lower limit of pyrolysis heights.

From figure 8 it can be seen that a power-law fit, $x_f = Bt^n$, with $n = 3/2$, agrees best with data, a conclusion further supported by the log-log plot and additional information given in the appendix.

5.4. Relationship between Flame and Pyrolysis Heights

Several upward-spread theories rely on a power-law correlation of flame height with pyrolysis height of the form $x_f \sim ax_p^m$ [27, 29, 30]. Figure 9 shows the ratio of the flame height to the pyrolysis height as a function of the heat-release rate. The lower heat-release rates occure at early times and are affected by the ignition process, which causes some pyrolysis as the flames develop. Soon, however, after that initial increasing period during which $\dot{Q}' < 15$ kW/m^2, the ratio of the flame height to the pyrolysis height appears to reach a steady value of approximately 1.4, corresponding to $m = 1$ in the preceding proportionality. The relationship of this observation to the other results is described below.

6. Discussion of Results and Physical Observations

Both flame and pyrolysis spread rates in this study fit most closely with a power-law relationship for corrugated cardboard, having a power lower than that often found for thermoplastic materials but higher than that sometimes inferred for wood, namely, we find $x_p \sim t^{3/2}$. The data are all mutually consistent in supporting this result. Our finding (section 2 and figure 6) that $x_f \sim \dot{Q}'$, within the accuracy of the data, is consistent with the results shown in figures 5 and 8 and with equations 9 and 10, with approximately, $B/A = 1.4$, according to figure 9. The resulting value of the ratio x_f/x_p that develops after the igntion period gives results very close to the average flame height of figure 5, when use is made of the pyrolysis height of figure 8, but appreciably less than the flame-tip height of figure 5, which correlates better with the literature results in figure 6. It becomes relevant, then, to ask why this corrugated cardboard behaves somewhat differently from other materials and exhibits lower average flame heights.

This difference appears to be mostly because the burning of this imperfect, cellulosic material, introduces complications in the burning process that are not considered in traditional models
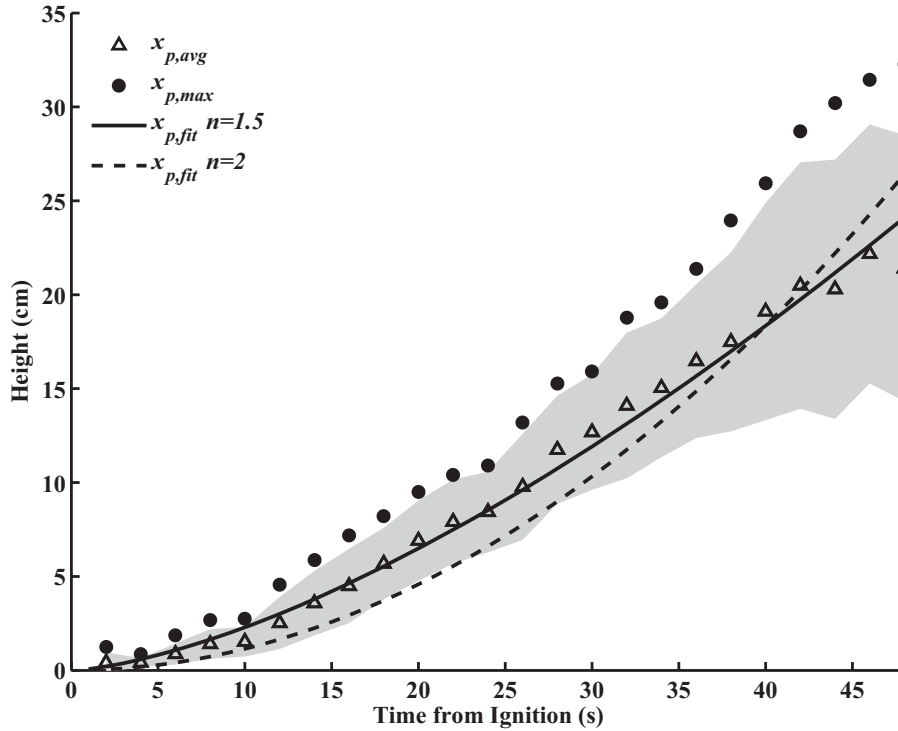
14

Figure 8: The pyrolysis front location, averaged over four experimental tests is shown as triangular points. A shaded gray region above and below the points indicate deviations between tests and across the width of the front face for each sampled point. Maximum pyrolysis heights are shown above the tip of the gray region, assessed as the maximum height of the pyrolysis front at a sampled time, averaged over four tests. Power-law fits to the average pyrolysis front, with time dependencies $n = 1.5$ and 2 are shown.

of flame spread. Observations from the side of spreading flames during the experiment reveal how differences from traditional similarity solutions may occur, namely through delamination of the top layer of fuel and its penetration into the boundary layer. Figure 10 shows a sample frame of corrugated cardboard with flames still residing on the front face. Unlike most thermoplastic fuels used in previous studies, and unlike more solid wood, corrugated cardboard is actually a two-layered fuel (figure 2) consisting of two layers of flat paper with a layer of corrugated paper in the center, glued and pressed together, leaving a significant air gap between the two flat layers. During experimentation, the front layer ignites first, followed by the back layer and inner material, which continues to smolder after progression of x_p. While the back layer of fuel is observed to remain intact throughout the duration of present experiments, the front layer rapidly burns off and delaminates from the corrugated and back layers, producing a "curling" effect on charred material, which physically disrupts the boundary layer above x_p. This may reduce the flame height over portions of the surface and thereby decrease the average flame height that is responsible for upward spread.

Emmons and Shen [48] observed a similar phenomenon when burning 10 cm high sheets of paper, where this charred residue of burnt paper curled upwards and penetrated the boundary layer. This process might be attributed to dual effects of pyrolysis leaving the top layer of the fuel
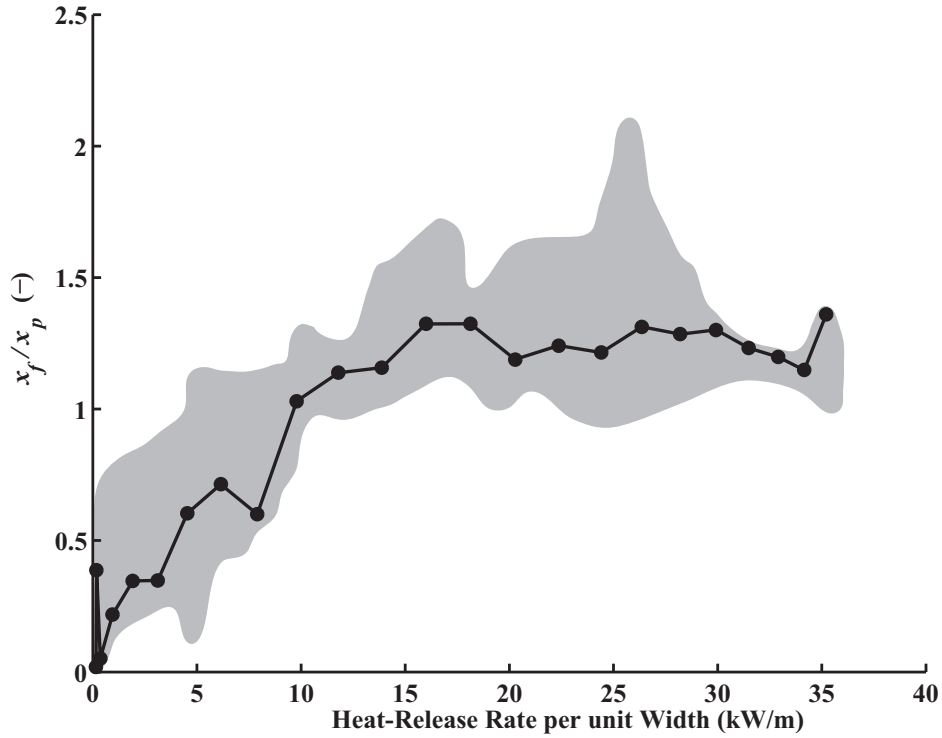
15

Figure 9: Ratio of the average flame height over pyrolysis height as a function of heat-release rate per unit width. Experimental scatter is indicated by a shaded gray region above and below averaged values.

sample adjacent to the flame much more rapidly than the inner layer, contracting the outer side and causing a slight curl (similar to what has been observed in experiments on matchsticks [49]), and the buoyant flow coming from burning material below then pushing this outer layer further outward and upward. This dual effect and the eventual hardening of charred residue produces a fairly solid obstruction that effectively increases the flame standoff distance past x_p, thereby decreasing the heat flux to the surface in a proportion to this extension. In order to reproduce the rates of spread observed in this study, a dependence of the flame standoff distance on height, $y_f \sim x^{1/3}$ was seen to correlate the data, but this can only represent an average effect since the resulting flow clearly is not self-similar. An interesting question concerns the extent to which this similarity behavior of the averages would extend to other materials at comparable stages of upward flame spread. While these results may have some degree of generality, the present work cannot address such questions, and so future studies employing other materials would be of great interest.

7. Conclusions

Despite many years of research, including the development of analytical and numerical models and extensive experimentation, the complexity of the process of upward flame spread continues to deserve attention in the fire-research community. Experiments performed in this study

Figure 10: *Left:* Front video footage during a representative test. The blue contour across the width indicates the measured height of the pyrolysis region. Image taken from the side of a sample during a representative test. Curling of the front layer of cardboard is visible in both images, but the extent of three-dimensional effects is more clearly seen in the side image.

focused on the most commonly used packaging material in warehouses, corrugated cardboard, which was found to affect predictions of upward flame spread by current descriptions. Physical disruptions in the boundary layer, produced by delamination of the top layer of corrugated cardboard, affects the heat flux ahead of x_p, for example by an increasing the average flame standoff distance. Many current flame-spread models employ a constant heat flux from the flame to unburnt surface, which may be inappropriate for the description of many different fuels at varying scales and which does not fit with a simplified description of the present observations. Instead, the spatial variation of the heat flux from the flame to the surface deserves further study for improved predictions in the future.

8. Acknowledgements

[1] C. M. Bidgood, P. F. Nolan, Warehouse fires in the UK involving solid materials, J. Loss Prev. Process Ind. 8 (1995) 11–16.
[2] C. D. Woodward, The industrial fire problem, Fire Saf. J. 15 (1989) 348–366.
[3] R. G. Zalosh, Industrial Fire Protection Engineering, John Wiley & Sons, New York, 2003.
[4] M. J. Gollner, K. Overholt, A. S. Rangwala, J. Perricone, F. A. Williams, Warehouse commodity classification from fundamental principles. Part I: Commodity and burning rates, Fire Saf. J. Under Review (2010).
[5] F. J. Kosdon, F. A. Williams, C. Buman, Combustion of vertical cellulosic cylinders, Proc. Combust. Inst. 12 (1969) 253–64.
[6] J. S. Kim, J. de Ris, F. W. Kroesser, Laminar free convective burning of fuel surfaces, Proc. Combust. Inst. 13 (1971) 949–961.
[7] M. Delichatsios, Surface extinction of flames on solids: Some interesting results, Proc. Combust. Inst. 31 (2007) 2749 – 2756.
[8] J. L. Torero, T. Vietoris, G. Legros, P. Joulain, Estimation of a total mass transfer number from the standoff distance of a spreading flame, Combust. Sci. Technol. 174 (2002) 187–203.
[9] P. J. Pagni, T. M. Shih, Excess pyrolyzate, Proc. Combust. Inst. 16 (1977) 1329–1343.

[10] K. Annamalai, M. Sibulkin, Flame spread over combustible surfaces for laminar flow systems Part I: Excess fuel and heat flux, Combust. Sci. Technol. 19 (1979) 167–183.

[11] T. Ahmad, G. M. Faeth, Turbulent wall fires, Proc. Combust. Inst. 17 (1978) 1149–1160.

[12] M. A. Delichatsios, Flame heights in turbulent wall fires with significant flame radiation, Combust. Sci. Technol. 39 (1984) 195–214.

[13] J. G. Quintiere, M. Harkleroad, Y. Hasemi, Wall flames and implications for upward flame spread, Combust. Sci. Technol. 48 (1986) 191–222.

[14] Y. Hasemi, Thermal modeling of upward wall flame spread, in: Fire Safety Science: Proceedings of the First International Symposium, International Association for Fire Safety Science, 1986, pp. 87–96.

[15] K. M. Tu, J. G. Quintiere, Wall flame heights with external radiation, Fire Technol. 27 (1991) 195–203.

[16] A. Tewarson, S. D. Ogden, Fire behavior of polymethylmethacrylate, Combust. Flame 89 (1992) 237 – 259.

[17] M. Coutin, J. M. Most, M. A. Delichatsios, M. M. Delichatsios, Flame heights in wall fires: effects of width, confinement and pyrolysis length, in: Fire Safety Science: Proceedings of the Sixth International Symposium, International Association for Fire Safety Science, 2000, pp. 729–740.

[18] M. Coutin, Etude Expérimentale et Théorique de lInfluence de lEntraînement dAir sur le Comportement dune Flamme Représentative dun Incendie, Ph.D. thesis, Université de Poitiers, France, 2000.

[19] K. C. Tsai, D. Drysdale, Upward flame spread: heat transfer to the unburned surface, in: Fire Safety Science: Proceedings of the Seventh International Symposium, International Association for Fire Safety Science, 2002, pp. 117–128.

[20] K. Tsai, D. Drysdale, Flame height correlation and upward flame spread modelling, Fire Mater. 26 (2002) 279–287.

[21] M. Delichatsios, Turbulent convective flows and burning on vertical walls, Proc. Combust. Inst. 19 (1983) 855–868.

[22] G. H. Markstein, J. de Ris, Upward fire spread over textiles, Proc. Combust. Inst. 14 (1973) 1085 – 1097.

[23] F. A. Williams, Combustion Theory, Westview Press, Menlo Park, CA, pg. 46, 1985.

[24] F. G. Roper, The prediction of laminar jet diffusion flame sizes: Part I. theoretical model, Combust. Flame 29 (1977) 219–226.

[25] A. C. Fernandez-Pello, T. Hirano, Controlling mechanisms of flame spread, Combust. Sci. Technol. 32 (1983) 1–31.

[26] B. Karlsson, Models for calculating flame spread on wall lining materials and the resulting heat release rate in a room, Fire Saf. J. 23 (1994) 365 – 386.

[27] L. Orloff, J. de Ris, G. H. Markstein, Upward turbulent fire spread and burning of fuel surface, Proc. Combust. Inst. 15 (1974) 183–192.

[28] A. C. Fernandez-Pello, A theoretical model for the upward laminar spread of flames over vertical fuel surfaces, Combust. Flame 31 (1978) 135 – 148.

[29] K. Annamalai, M. Sibulkin, Flame spread over combustible surfaces for laminar flow systems Part II: Flame heights and fire spread rates, Combust. Sci. Technol. 19 (1979) 185–193.

[30] K. Saito, J. G. Quintiere, F. A. Williams, Upward turbulent flame spread, in: Fire Safety Science: Proceedings of the First International Symposium, International Association for Fire Safety Science, 1985, pp. 75–86.

[31] H. E. Mitler, Predicting the spread rates of fires on vertical surfaces, Proc. Combust. Inst. 23 (1991) 1715–1721.

[32] Y. Hasemi, M. Yoshida, A. Nohara, T. Nakabayashi, Unsteady-state upward flame spreading velocity along vertical combustible solid and influence of external radiation on the flame spread, in: Fire Safety Science: Proceedings of the Third International Symposium, International Association for Fire Safety Science, 1991, pp. 197–206.

[33] G. Grant, D. Drysdale, Numerical modelling of early flame spread in warehouse fires, Fire Saf. J. 24 (1995) 247 – 278.

[34] K. Saito, F. A. Williams, L. Wichman, J. G. Quintiere, Upward turbulent flame spread on wood under external radiation, J. Heat Transfer (1989).

[35] M. Sibulkin, J. Kim, The dependence of flame propagation on surface heat transfer II. Upward burning, Combust. Sci. Technol. 17 (1976) 39–49.

[36] J. Consalvi, Y. Pizzo, B. Porterie, Numerical analysis of the heating process in upward flame spread over thick pmma slabs, Fire Saf. J. 43 (2008) 351 – 362.

[37] W. Xie, P. E. DesJardin, An embedded upward flame spread model using 2d direct numerical simulations, Combust. Flame 156 (2009) 522 – 530.

[38] A. S. Rangwala, S. G. Buckley, J. L. Torero, Upward flame spread on a vertically oriented fuel surface: The effect of finite width, Proc. Combust. Inst. 31 (2007) 2607–2615.

[39] Y. Pizzo, J. L. Consalvi, P. Querre, M. Coutin, B. Porterie, Width effects on the early stage of upward flame spread over pmma slabs: Experimental observations, Fire Saf. J. 44 (2009) 407 – 414.

[40] K. C. Tsai, F. S. Wan, Upward flame spread: the width effect, in: Fire Safety Science: Proceedings of the Eighth International Symposium, International Association for Fire Safety Science, 2005, pp. 409–419.

[41] K. C. Tsai, Width effect on upward flame spread, Fire Saf. J. 44 (2009) 962 – 967.

[42] T. M. Jayaweera, H.-Z. Yu, Water absorption in horizontal corrugated boards under water sprays, Fire Saf. J. 41
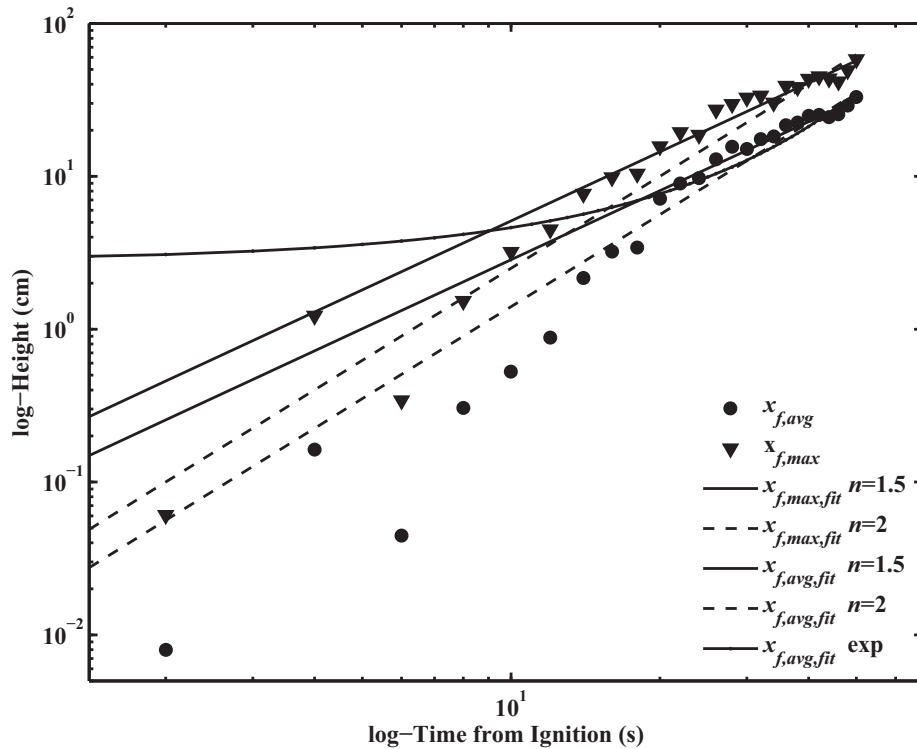
Figure 11: log-Time versus log-Height plot of the average and maximum flame heights with several possible power-law fits shown. A power-law fit with $n = 1.5$ closely represents both maximum and average flame height data. Circles denote averaged flame height locations between all four tests, and dots averaged values from each experiment. An exponential fit to the data does not fit experimental data well.

(2006) 335 – 342.

[43] L. Audouin, G. Kolb, J. L. Torero, J. M. Most, Average centreline temperatures of a buoyant pool fire obtained by image processing of video recordings, Fire Saf. J. 24 (1995) 167 – 187.

[44] J. L. Consalvi, Y. Pizzo, B. Porterie, J. L. Torero, On the flame height definition for upward flame spread, Fire Saf. J. 42 (2007) 384 – 392.

[45] M. J. Gollner, A Fundamental Approach to Commodity Classification, Master's thesis, University of California, San Diego, La Jolla, CA, 2010.

[46] A. Tewarson, Generation of heat and gaseous, liquid, and solid products, in: P. J. DiNenno (Ed.), SFPE Handbook of Fire Protection Engineering, Fourth Edition, National Fire Protection Association, 2008, pp. 3–(109–194).

[47] A. Arakawa, K. Saito, W. A. Gruver, Automated infrared imaging temperature mesaurements with application to upward flame spread studies. Part I, Combust. Flame 92 (1993) 222–230.

[48] H. W. Emmons, T. Shen, Fire spread in paper arrays, Proc. Combust. Inst. 13 (1971) 917 – 926.

[49] M. Vogel, F. A. Williams, Flame propagation along matchstick arrays, Combust. Sci. Technol. 1 (1970) 429–436.

Appendix A. Additional Fits to Experimental Data

Figures 11 and 12 show log-log plots of data in figures 5 and 8, respectively, including exponential as well as power-law fits. These plots provide greater separation of different predictions and so help in selecting the best results. The exponent, n for fits to average flame and pyrolysis
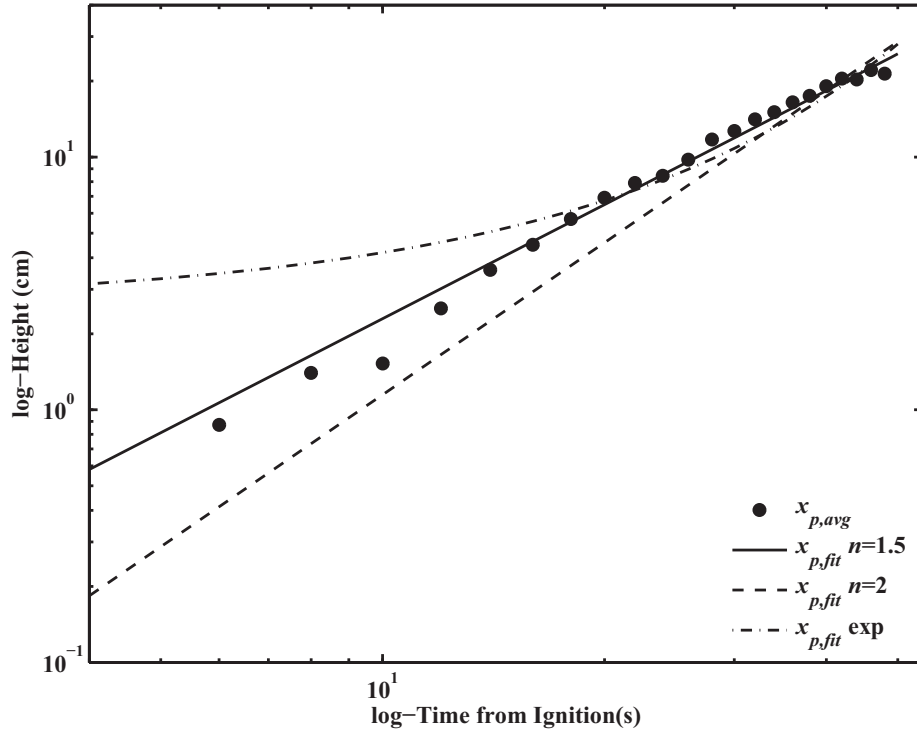
Figure 12: log-Time versus log-Height plot of the pyrolysis height with several possible fits to the function is shown. The best fit to the data appears to be a power-law fit close to n=1.5. Circles denote averaged pyrolysis locations between all four tests, and dots averaged values from each experiment. An exponential fit to the data does not fit experimental data well.

heights was found to lie between $n = 1.4$–1.8 for average flame heights, between $n = 1.1$–1.5 for maximum flame heights, and $n = 1.3$–1.5 for pyrolysis heights within a 95% confidence interval. Therefore, the selection of $n = 1.5$ was deemed the most reasonable value to use in analysis, as it lies within the 95% confidence intervals of all measured data. Exponential fits are provided here in figures 11 and 12 to illustrate their poor fit, but they were not included in figure 5 and 8 because they did not represent the data well.

A summary of least-squares fits applied to experimental data is provided in table 1. Coefficients for power-law fits to averaged experimental data are shown along with R^2 values representing the goodness-of-fit. Best-fits, as found by a least-squares fitting algorithm as well as fits to specific powers, $n = 1.5, 2, 3$ are provided for reference.

Fit	n	A	R^2
$x_{f,avg}$ best fit	1.6	0.062	0.97
$x_{f,avg}$ fit	1.5	0.090	0.97
$x_{f,avg}$ fit	2	0.014	0.95
$x_{f,avg}$ fit	3	0.00032	0.80
$x_{f,max}$ best fit	1.4	0.28	0.97
$x_{f,max}$ best	1.5	0.16	0.97
$x_{f,max}$ fit	2	0.025	0.90
$x_{f,max}$ fit	3	0.00056	0.67
$x_{p,avg}$ best fit	1.4	0.10	0.99
$x_{p,avg}$ fit	1.5	0.073	0.99
$x_{p,avg}$ fit	2	0.011	0.93
$x_{p,avg}$ fit	3	0.00027	0.71

Table 1: Coefficients of least-squares fits applied to experimental flame and pyrolysis heights data, where x_p and x_f are in cm. Power-law fits are shown, of the form $x = At^n$. Exponential fits are not shown because they were all far beyond acceptable error limits.